Biomaterials 35 (2014) 6078–6085

Contents lists available at ScienceDirect

Biomaterials

journal homepage: www.elsevier.com/locate/biomaterials

# Live cells imaging using a turn-on FRET-based BODIPY probe for biothiols

Dongdong Su [a], Chai Lean Teoh [a], Srikanta Sahu [a], Raj Kumar Das [a], Young-Tae Chang [a,b,*]

[a] Department of Chemistry and MedChem Program, Life Sciences Institute, National University of Singapore, 3 Science Drive 3, Singapore 117543, Singapore
[b] Laboratory of Bioimaging Probe Development, Singapore Bioimaging Consortium (SBIC), 11 Biopolis Way, #02-02 Helios, Agency for Science, Technology and Research (A*STAR), Biopolis, Singapore 138667, Singapore

ARTICLE INFO

*Article history:*
Received 6 March 2014
Accepted 11 April 2014
Available online 1 May 2014

*Keywords:*
Fluorescence
Fluorescence resonance energy transfer (FRET)
Biothiols
cysteine
Sensor

ABSTRACT

We designed a red-emitting turn-on FRET-based molecular probe **1** for selective detection of cysteine and homocysteine. Probe **1** shows significant fluorescence enhancement after cleavage of the 2, 4-dinitrobenzensulfonyl (DNBS) unit from the fluorophore upon thiols treatment. The precursor of probe **1**, **BNM153**, is a moderate quantum yield FRET dye which contributes a minimum emission leakage from its donor part. We synthesized this assembly by connecting a low quantum yield (less than 1%) BODIPY donor to a high quantum yield BODIPY acceptor via a 1, 3-triazine bridge system. It is noteworthy that the majority of the non-radiative energy loss of donor (**BDN**) was converted to the acceptor (**BDM**)'s fluorescence output with minimum leaks of donor emission. The fluorescence sensing mechanism of probe **1** was illustrated by fluorescence spectroscopy, kinetic measurements, HPLC-MS analysis and DFT calculations. Probe **1** is pH-independent at the physiological pH range. Finally, live cells imaging demonstrated the utility of probe **1** as a biosensor for thiols.



## 1. Introduction

Biological thiols such as cysteine (Cys), homo-cysteine (Hcy), and glutathione (GSH) play important roles in a number of biological processes in living organisms [1,2]. Cys is precursor to the antioxidant GSH, and their abnormal levels are closely related to human ageing and various diseases [3]. While Hcy is a risk factor for Alzheimer's disease and cardiovascular diseases, total plasma Hcy concentrations have been proven to link to birth defects and cognitive impairment at the elderly stage [4]. In view of the importance of thiols, the design of analytical methodologies for the detection of biomolecular thiols in biological and environmental samples has consistently attracted a great deal of attention. Traditional detection methods such as high performance liquid chromatography (HPLC) [5], electrophoresis-based methods [6], as well as electrospray ionization-mass spectrometry [7] have been used to detect thiols. However, these methods are not convenient for use, since they often involve the expensive instrumentation and can be technically demanding in their handling.

On the contrary, fluorescent molecular probes are more attractive, due to their high sensitivity and easy visibility. Also, fluorescent molecular probes offer the possibility of quantitative optical detection of biothiols and broad bioimaging applications, such as detecting the carcinoma region of liver tissue based on the differences of glutathione level [8]. Till now, a number of diverse sensing mechanisms have been employed for thiol detection, including thiol–halogen nucleophilic substitution [9,10], Michael addition [11–14], –CHO attached fluorophores [15–18], and de-protection of 2,4-dinitrobenzenesulfonyl (DNBS)-protected fluorophores [19–24]. Most of these published probes show good selectivity and sensitivity in detecting certain biothiols by simple spectroscopic techniques, which monitor optical responses caused by different concentrations of biothiols. However, most of them were designed based on a single fluorophore as the fluorescence signalling profile, which may limit their applications. These single fluorophore probes have small Stokes shifts, which can lead to serious self-quenching and fluorescence detection error due to excitation backscattering effects. Some FRET-based probes, constructed with dyes that have high extinction coefficients and high quantum yields as donors, have also been explored for thiols detection. Unfortunately, instances of fluorescence leaks from the donor have been inevitable, as a result of either low energy transfer efficiencies or environmental changes [25,26].

* Corresponding author. Department of Chemistry and MedChem Program, Life Sciences Institute, National University of Singapore, 3 Science Drive 3, Singapore 117543, Singapore.
*E-mail address:* chmcyt@nus.edu.sg (Y.-T. Chang).

http://dx.doi.org/10.1016/j.biomaterials.2014.04.035
0142-9612/

Hence, newly improved FRET probes with better photophysical properties, which can efficiently eliminate the interference from background fluorescence and scattered light, are worthwhile to design. Several criteria must be satisfied for the FRET probe: 1) absorbance of light at a high extinction coefficient but no fluorescence emission from donor part to ensure that there is no background influence; 2) large pseudo-Stokes shifts and emission shifts to avoid serious self-quenching and fluorescence detection errors caused by excitation backscattering effects [27,28]; 3) high efficient FRET energy transfer. Here, we designed and synthesized a turn-on FRET-based molecular probe **1** containing a 2,4-dinitrobenzenesulfonyl (DNBS) group on its acceptor, acting as the reaction site for biothiols. In addition, the application of probe **1** for sensing thiols in live cells and its sensing mechanism were also investigated.

## 2. Experimental section

### 2.1. Materials

The chemicals and solvents, were purchased from Sigma Aldrich, Acros and Alfa Aesar. All the chemicals were directly used without further purification. Normal phase column chromatography purification was carried out using MERCK silica Gel 60 (Particle size: 230–400 mesh, 0.040–0.063 mm).

### 2.2. Measurements and analysis

HPLC-MS was taken on an Agilent-1200 with a DAD detector and a single quadrupole mass spectrometer (6130 series). The analytical method, unless indicated, is A: $H_2O$ (0.1% HCOOH), B: $CH_3CN$ (0.1% HCOOH), gradient from 10 to 90% B in 10 min; C18 (2) Luna column (4.6 × 50 $mm^2$, 3.5 μm particle size).

Spectroscopic and quantum yield data were measured on a SpectraMax M2 spectrophotometer (Molecular Devices). Data analysis was performed using GraphPrism 5.0.

$^1H$ NMR and $^{13}C$ NMR spectra were recorded on Bruker ACF300 (300 MHz) or AMX500 (500 MHz) spectrometers, and chemical shifts are expressed in parts per million (ppm) and coupling constants are reported as a *J* value in Hertz (Hz).

### 2.3. Quantum yield measurements

Quantum yields for all the fluorescent compounds were measured by dividing the integrated emission area of their fluorescent spectrum against the area of Rhodamine B in EtOH excited at 490 nm ($\Phi_{rho\text{-}B} = 0.7$) [29]. Quantum yields where then calculated using equation (1), where *F* represents the integrated emission area of fluorescent spectrum, $\eta$ represents the refractive index of the solvent, and Abs represents absorbance at excitation wavelength selected for standards and samples. Emission was integrated from 530 nm to 750 nm.

$$\Phi_{flu}^{sample} = \Phi_{flu}^{sample}\left(\frac{F^{sample}}{F^{reference}}\right)\left(\frac{\eta^{sample}}{\eta^{reference}}\right)\left(\frac{Abs^{reference}}{Abs^{sample}}\right) \quad (1)$$

### 2.4. DFT calculations

All calculations have been performed with the Gaussian 09 code. Full geometry optimizations and electronic structure calculations were performed with density functional theory (DFT) at B3LYP/6-31G(d) level. The excited state related calculations were carried out with the time-dependent DFT (TDDFT), based on the optimized ground state geometry [30].

### 2.5. Cell culture and imaging experiments

HeLa cells were cultured in clear bottom, 96-well plate and maintained in an incubator at 37 °C with 5% $CO_2$, 24–36 h prior to imaging experiments. Cells were grown in Dulbecco's Modified Eagle Medium (Sigma) with 10% newborn calf serum, as well as 5 mM L-glutamine and 5 mg/mL gentamicin. Probe stock solution in DMSO (1 mM) was diluted to 100 μM with PBS before being added to cell culture wells to reach the final concentration of 3 μM. After 30 min incubation at 37 °C, cells were washed with PBS buffer twice prior to imaging. Cells were also treated with 1 mM N-methylmaleimide in PBS at 37 °C for 30 min and subsequently washed twice with PBS buffer, prior to incubation with probe as per described. Separately, as control experiment, cells were pre-treated with 1 mM L-buthionine sulfoximine (BSO) or 1 mM BSO in the presence of 0.1 mM hydrogen peroxide for 1 h. The latter was further treated with 1 mM L-cysteine for 1 h or left untreated before incubation with probe. Live cells imaging was done with an inverted fluorescence microscope Ti (Nikon), equipped with an Ex 480 nm/40, long-pass 510 nm filter for fluorescence image acquisition.

### 2.6. Synthesis

The **BDN** and **BDM153** were synthesized following our previous report [31,32].

#### 2.6.1. Synthesis of ***BDN-Tri***

To a solution of **BDN** (115 mg, 0.37 mmol) in 70 mL of dry tetrahydrofuran (THF) was added cyanuric chloride (101 mg, 0.55 mmol). The reaction mixture was stirred for 1 h at 0 °C. After removal of the THF, the residue was purified by silica gel chromatography (hexane–EtOAc, 4:1) to give **BDN-Tri** as a yellow solid (152 mg, 90%).

$^1H$ NMR (300 MHz, $CDCl_3$): δ 7.81 (s, 1H), 7.73 (d, *J* = 8.5 Hz, 2H), 7.70 (s, 1H), 7.40 (d, *J* = 8.5 Hz, 2H), 6.41 (s, 1H), 6.38 (s, 1H), 6.15 (s, 1H), 2.63 (s, 3H), 1.60 (s, 3H); $^{13}C$ NMR (75.5 MHz, $CDCl_3$): 171.47, 170.44, 164.02, 162.37, 146.68, 142.13, 138.89, 137.22, 134.56, 133.51, 130.92, 129.95, 126.91, 123.41, 120.48, 116.20, 29.65, 15.24.

HRMS *m/z* ($C_{20}H_{15}BCl_2F_2N_6$) calculated $(M-H)^-$: 457.0718, found $(M-H)^-$: 457.0716.

#### 2.6.2. Synthesis of ***BDM153***

Compound **2** (50 mg, 103 μmol) and 4-hydroxybenzaldehyde (25.2 mg, 206 μmol) were dissolved in acetonitrile (5 mL), with pyrrolidine (5.2 μL, 618 μmol) and 6 equiv. of AcOH (3.5 μL, 618 μmol). The mixture was heated to 85 °C and keep for 5 min. After removal of the solvent, the residue was purified by silica gel chromatography (eluents: $CH_2Cl_2$–MeOH, 98: 2 to 90: 10) to give **BDM153** as a purple solid (21.7 mg, 57%).

$^1H$ NMR (500 MHz, $CDCl_3$): δ 7.38 (s, 1H), 7.30 (d, *J* = 8.6 Hz, 2H), 7.24 (dd, *J* = 34.7, 16.3 Hz, 3H), 7.09 (d, *J* = 3.8 Hz, 1H), 6.66 (s, 1H), 6.68 (d, *J* = 8.5 Hz, 2H), 6.65 (dd, *J* = 3.9, 2.1 Hz, 1H), 3.22–3.19 (m, 2H), 3.01–2.98 (m, 2H), 2.34 (s, 3H); $^{13}C$ NMR (125 MHz, $CDCl_3$):159.32, 159.19, 144.21, 141.47, 136.46, 135.46, 135.14, 133.37, 129.74, 127.21, 122.03, 120.12, 115.71, 115.60, 114.69, 44.98, 23.80, 15.70.

HRMS *m/z* ($C_{20}H_{20}BF_2N_3O$) calculated $(M+Na)^+$: 390.1565, found $(M+Na)^+$: 390.1573.

#### 2.6.3. Synthesis of ***BNM153***

**BDN-Tri** (20 mg, 54 μmol), **BDM153** (25 mg, 54 μmol) and DIEA (14 μL, 108 μmol) were dissolved in THF (10 mL) and stirred at room temperature for 2 h. After evaporation of the solvent, the crude product was purified by silica gel chromatography (eluents: $CH_2Cl_2$ to $CH_2Cl_2$–MeOH (95: 5)) to afford the corresponding **BNM153** as red solid (30.7 mg, 72%).

$^1H$ NMR (500 MHz, $CD_3CN$): δ 8.21 (d, *J* = 11.6 Hz, 1H), 7.88 (d, *J* = 8.3 Hz, 1H), 7.72 (d, *J* = 8.2 Hz, 1H), 7.66 (s, 1H), 7.58 (d, *J* = 10.1 Hz, 1H), 7.55 (d, *J* = 8.4 Hz, 1H), 7.49 (d, *J* = 8.6 Hz, 1H), 7.44–7.40 (m, 2H), 7.32 (d, *J* = 8.2 Hz, 1H), 7.19 (s, 1H), 6.97–6.89 (m, 3H), 6.51–6.44 (m, 3H), 6.27 (d, *J* = 47.5 Hz, 1H), 3.83 (dd, *J* = 13.5, 6.8 Hz, 1H), 3.70 (dd, *J* = 14.8, 7.1 Hz, 1H), 3.32 (dd, *J* = 13.7, 6.7 Hz, 2H), 2.63–2.52 (m, 6H), 1.62 (d, *J* = 41.6 Hz, 3H); $^{13}C$ NMR (125 MHz, $CD_3CN$): 166.14, 164.40, 162.58, 159.10, 147.71, 145.81, 143.61, 143.45, 141.08, 140.72, 140.51, 140.42, 140.12, 139.81, 137.85, 137.77, 136.40, 136.17, 133.63, 129.72, 129.64, 129.59, 128.48, 127.91, 126.65, 126.54, 123.67, 123.57, 123.37, 120.26, 119.91, 119.75, 116.05, 116.02, 114.95, 42.16, 29.80, 15.96, 15.80, 14.34.

HRMS *m/z* ($C_{40}H_{34}B_2ClF_4N_9O$) calculated $(M-H)^-$: 788.2619, found $(M-H)^-$: 788.2610.

#### 2.6.4. Synthesis of probe ***1***

**BNM153** (30 mg, 38 μmol) and $Et_3N$ (16 μL, 114 μmol) was dissolved in 10 mL of dry $CH_2Cl_2$. The mixture was stirred at 0 °C for 15 min under $N_2$ atmosphere. A solution of 2,4-dinitrobenzenesulfonyl chloride (20.3 mg, 76 μmol) in 5 mL $CH_2Cl_2$ was added dropwise. The reaction mixture was stirred for 2 h at rt. After evaporation of the solvent, the crude product was purified by silica gel chromatography (eluents: $CH_2Cl_2$ to $CH_2Cl_2$–MeOH (95: 5)) to afford the corresponding probe **1** as red solid (23 mg, 59%).

$^1H$ NMR (500 MHz, $CDCl_3$): δ 8.66 (s, 1H), 8.48 (d, *J* = 8.6 Hz, 1H), 8.14 (dd, *J* = 8.6, 4.9 Hz, 1H), 7.72 (d, *J* = 8.4 Hz, 1H), 7.63–7.48 (m, 7H), 7.33 (d, *J* = 3.6 Hz, 1H), 7.27–7.15 (m, 4H), 6.48–6.34 (m, 3H), 6.10 (d, *J* = 21.9 Hz, 1H), 3.80 (s, 1H), 3.68 (s, 1H), 3.26 (dd, *J* = 15.0, 7.5 Hz, 2H), 2.58–2.43 (m, 6H), 1.55 (d, *J* = 28.0 Hz, 3H); $^{13}C$ NMR (125 MHz, $CDCl_3$): 165.28, 162.12, 161.97, 155.68, 155.58, 150.90, 149.01, 148.82, 146.82, 139.09, 138.93, 138.75, 138.36, 138.25, 136.64, 136.56, 135.91, 135.80, 134.59, 133.91, 133.88, 133.47, 133.10, 129.52, 129.44, 129.20, 126.84, 126.50, 126.45, 124.56, 123.35, 123.23, 122.36, 122.32, 120.29, 120.11, 120.01, 119.90, 119.50, 116.64, 116.56, 115.95, 42.44, 30.72, 16.42, 14.93.

HRMS *m/z* ($C_{46}H_{36}B_2ClF_4N_{11}O_7S$) calculated $(M-H)^-$: 1018.2252, found $(M-H)^-$: 1018.2230.

## 3. Results and discussion

### 3.1. Design and synthesis of the probe 1

Here, we designed a reactive FRET probe **1** having long emission wavelength and large pseudo-Stokes shifts characteristics. **BDN** skeleton was chosen as the donor because of its high extinction coefficient and low quantum efficiency [32]. The red emitting styryl **BDM153** was chosen as acceptor part of the FRET pair of probe **1**,

which is expected to be a good quantum yield BODIPY dye with emission at 580 nm. This elegant choice of donor and acceptor, when successfully incorporated into a triazine- moiety results in a large Stokes-shifts dye, the precursor of probe **1**, which has moderate quantum yield with minimum emission leakage from donor part. This precursor of probe **1**, **BNM153**, consists of hydroxyl group at the end of **BNM** acceptor, which is reasoned to be a high quantum yield dye. Upon obtaining the large Stokes-shifts, FRET based-precursor, the strong electron-deficient 2,4-dinitrobenzenesulfonyl group (DNBS), was introduced at the end of probe **1**, hoping that it would give rise to a fluorogenic thiol reactive probe **1**. Here the fluorogenic characteristic or in other word the reduction of fluorescence intensity is caused by the intramolecular photoinduced electron transfer (PeT) process from the excited fluorophore to the strong electron-acceptor DNBS. Based on previous knowledge, it is evident that after the addition of Cys or Hcy to probe **1**, reaction would occur to cleave DNBS quencher from the probe **1** and thereby emission would restore. The major advantage of this current thiol probe over the existing FRET probes would be the minimum emission leakage from the donor site. In general, upon binding to the analyte, emission leakage from the donor site is quite inevitable for the regular FRET probe and thereby it limits the possibility of usage of probe as multicolour imaging agent. Therefore, this is the first report of a turn on red-emitting FRET based biothiol probe where there is no emission leakage from the donor site of the probe.

Scheme 1 indicates the synthesis of probe **1**. At first, **BDN** was reacted with the cyanuric chloride linker to obtain an intermediate **BDN-Tri**. Then, this key intermediate was reacted with acceptor **BDM153** to give a FRET construct **BNM153**. A DNBS group was then incorporated to **BNM153** in the presence of $Et_3N$ to get the target probe **1**. Since the DNBS unit is known to be a potent electron acceptor which produces a dark excited state, the incorporation of this unit into the fluorescent molecule (**BNM153**) would consequently quench the emission to give probe **1**, a non-fluorescent thiol reactive dye. Subsequent cleavage of the DNBS group will then restore the emission of the fluorophore **BNM153** in the

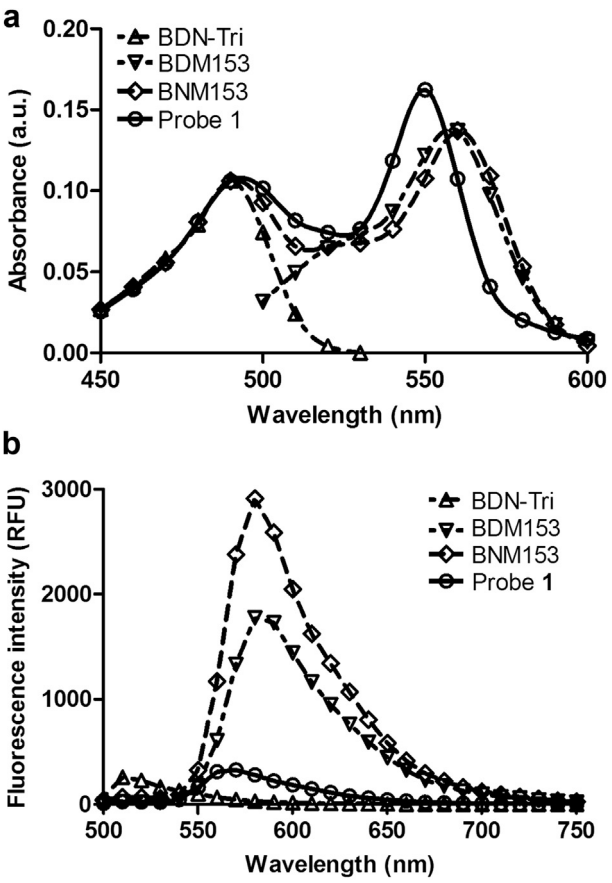


**Fig. 1.** The absorbance and emission spectra of probe **1** and the relative compounds (10 μM in MeOH–$H_2O$, 4:1, v/v, $\lambda_{ex}$ = 470 nm).

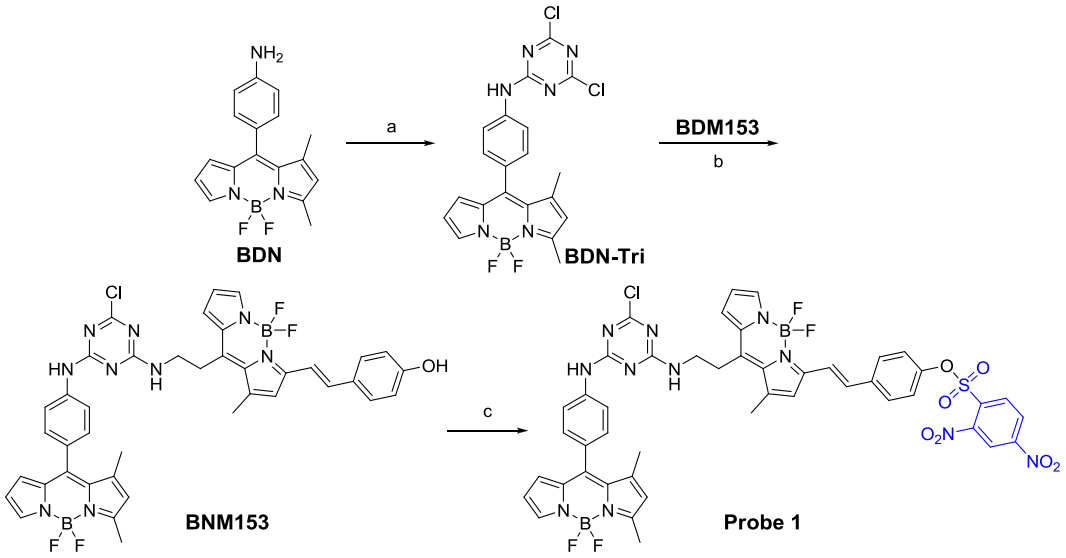


Reagents and conditions: (a) Cyanuric chloride, DIEA, THF, 0 ºC, 1h; (b) DIEA, THF, rt, 2h; (c) 2,4-Dinitrobenzenesulfonyl chloride, $Et_3N$, DCM, rt, 2 h.

**Scheme 1.** Synthesis of the FRET thiol probe **1**.

**Table 1**
Photophysical data of **BDN-Tri**, **BDM153**, precursor **BNM153** and probe **1** (MeOH–$H_2O$, 4:1, v/v).

| | $\lambda_{abs}$ (nm)[a] | Log $\varepsilon_{max}$ | $\lambda_{abs}$ (nm)[b] | Log $\varepsilon_{max}$ | $\lambda_{em}$ (nm) | $\Phi$[c] | $\Delta\lambda$[d] |
|---|---|---|---|---|---|---|---|
| **BDN-Tri** | 492 | 4.65 | – | – | 510 | <0.001 | 18 |
| **BDM153** | – | – | 560 | 4.76 | 580 | 0.56 | 20 |
| **BNM153** | 494 | 4.66 | 561 | 4.76 | 580 | 0.16 | 86 |
| Probe **1** | 494 | 4.66 | 551 | 4.83 | 561 | 0.01 | 67 |

[a] The maximal absorption of donor part.
[b] The maximal absorption of acceptor part.
[c] Fluorescence quantum yields were determined using rhodamine B ($\Phi_f = 0.7$ in EtOH) as a standard [29].
[d] Pseudo-Stokes shifts of the **BNM153** and probe **1** and the Stokes shifts of the **BDN-Tri** and **BDM153**.

presence of thiols. The structures were fully characterized by $^1$H NMR, $^{13}$C NMR and HRMS analysis.

### 3.2. Spectroscopic properties of compounds

The absorbance and fluorescence spectra of probe **1**, the precursor **BNM153**, **BDN-Tri** and **BDM153** were investigated. The absorption spectra of **BNM153** displayed the characteristic absorption signal of **BDN-Tri** at around 494 nm and the typical absorption signal of **BDM153** at around 561 nm, respectively (Fig. 1a). Compared with the unconjugated **BDN-Tri** and **BDM153**, the shape of **BNM153** absorption spectra did not show obvious change, which reveals that the electronic interactions between the donor and the acceptor are very weak. Compared with the precursor **BNM153**, absorption of probe **1** shows a blue shift, due to the protection of the strong electron-acceptor DNBS. The emission spectra of probe **1** and its precursor **BNM153** are shown in Fig. 1b. Upon excitation of probe **1** at the donor absorption band (470 nm), only the characteristic emission band of the acceptor at around 561 nm was observed, while the emission of **BDN-Tri** was not observed. This indicates that the energy transfer is efficient from donor to acceptor. For **BNM153**, the maximum emission wavelength was shifted to 580 nm. It is worth noting that the quantum yield of **BNM153** is much larger than probe **1**, which is almost non-fluorescent because of the PeT process. The maximum wavelengths of absorbance, fluorescence emission, quantum yield, and Stokes shifts as discussed above are summarized in Table 1.

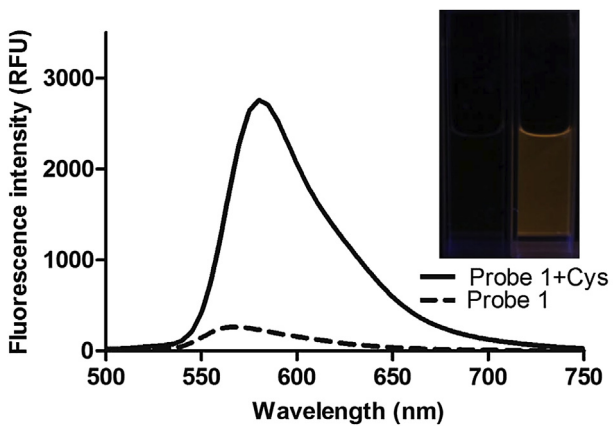


**Fig. 2.** Fluorescence emission spectra ($\lambda_{ex}$ = 470 nm) of probe **1** (10 μM) before and after addition of L-cysteine (3 mM, MeOH–$H_2O$, 4:1, v/v). Inset: Pictures of probe **1** (10 μM) before and after adding L-cysteine (3 mM) under irradiation with a hand-held 365 nm lamp.

### 3.3. Selective detection of Cys and Hcy

The fluorescence response of probe **1** towards Cys was investigated. The pH-independent spectra shows that probe **1** can work in a wide physiological pH range (Fig. S1 in the Supporting Information). All the tests were taken 1 h after the addition of Cys, to ensure that the reaction reached equilibrium. Probe **1** alone is almost non-fluorescent, as a result of the quenching effect of the protecting group DNBS. In the presence of Cys, however, the electro-withdrawing DNBS moiety is cleaved and the fluorescence intensity is dramatically enhanced by 12-fold at 580 nm. Also, a remarkable red shift of the maximum emission (19 nm) between probe **1** and the corresponding cleavage **BNM153** and a large pseudo-Stokes shift were observed. After cleavage, the precursor **BNM153** displays an intense absorption at 494 nm and emission at 580 nm, giving a pseudo-Stokes shifts of up to 86 nm. In addition, the emission colour changed from non-fluorescent to bright orange, which corresponds to probe **1** and **BNM153** after the addition of Cys (Fig. 2). Also, emission spectra of probe **1** show that this is no emission leakage from donor part before and after addition of Cys, clearly demonstrating its advantage over other FRET dyes in their applications.

Under optimal conditions, we evaluated the capability of the proposed method for quantitative detection of Cys. The fluorescence responses of probe **1** with different concentrations of Cys (0–4 mM) are shown in Fig. 3. The results show that the fluorescence of probe **1** increases with gradual addition of Cys (0–4 mM). A linear

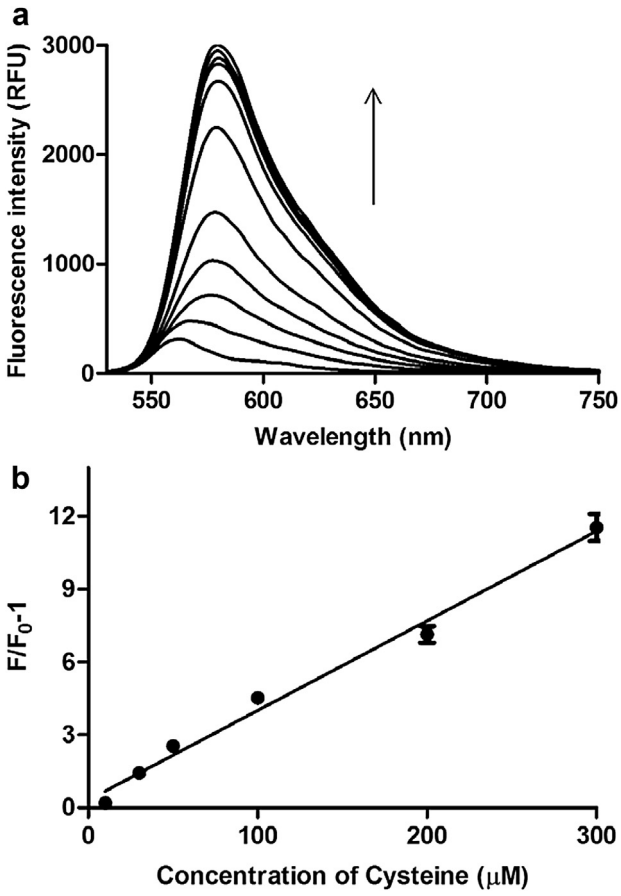


**Fig. 3.** (a) Fluorescence response of probe **1** (10 μM) upon incubation with serial dilutions of Cys (0–4 mM) ($\lambda_{ex}$ = 490 nm); (b) A linear relationship of the fluorescence intensity *vs.* the concentration of Cys (0–300 μM) Values are represented as means ($n$ = 3). Measurements were taken at rt.

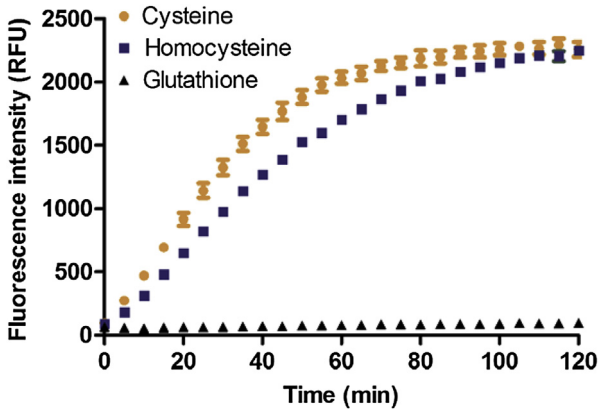


**Fig. 4.** The sensing kinetics of probe **1** (10 μM) toward Cys, Hcy and GSH (3 mM). $\lambda_{ex}$ = 490 nm, $\lambda_{em}$ = 580 nm. Values are represented as means and error bars as standard deviations ($n$ = 3). Measurements were taken at rt.

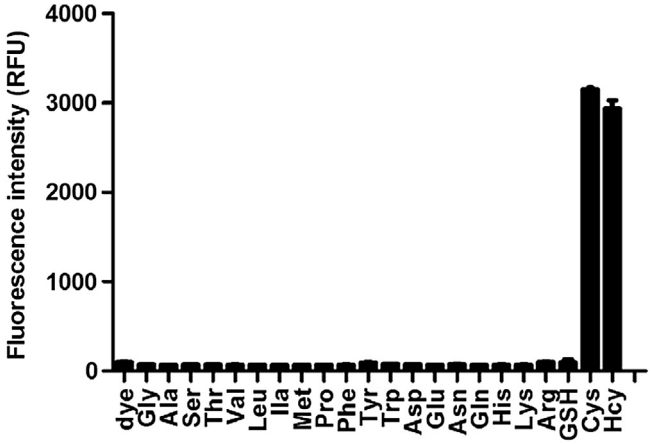


**Fig. 5.** Fluorescence responses of probe **1** (10 μM) to different analytes (3 mM). Values are represented as means and error bars as standard deviations ($n$ = 3). Measurements were taken at rt.

increment, with respect to the concentration of Cys within the 0–0.3 mM range, is also observed. The calculated $K_d$ value for Cys is 0.37 mM (Fig. S2 in the Supporting Information).

The sensing kinetics of Cys, Hcy and GSH by probe **1** was also investigated. As shown in Fig. 4, the recognition of Cys and Hcy by probe **1** almost complete within 60 min, whereas probe **1** does not show any observed response towards GSH. Reaction rate constants for the recognition of Cys and Hcy were determined to be 0.027 $min^{-1}$ and 0.016 $min^{-1}$, respectively (Fig. S3 in the Supporting Information). The results obtained in this study are consistent with the reported Cys probes based on the same mechanism design [23,25].

In order to examine the selectivity of probe **1**, the fluorescence change of probe **1** in the presence of different amino acids and biological thiols, such as GSH and Hcy, was examined by monitoring the changes in emission spectral intensities at 580 nm. The results of the fluorescence changes are summarized in Fig. 5. Probe **1** shows good selectivity for Cys and Hcy over other amino acids. At the same time, probe **1** also displays very weak response towards GSH, which is probably due to the bulkiness of this analyte in the solvent system [23,25]. Therefore, the probe **1** is highly selective towards Cys and Hcy.

### 3.4. Rationalization of the sensing mechanism of thiol probe

The selectivity of probe **1** is dependent on its sensing mechanism. Although the mechanism of detecting Cys using similarly designed dyes has been studied by NMR and HRMS, no systematic study regarding the change of reaction in aqueous media has been reported to date [24,33]. To obtain more detailed insights into the mechanism, interaction between probe **1** and Cys was monitored by HPLC-MS. Results from HPLC-MS monitor test show that the signal corresponding to probe **1** at 8.3 min became smaller, whereas a new peak corresponding to **BNM153** at 8 min appeared and got bigger over time (Fig. 6). This result was further confirmed by mass spectra analysis. The signal at 8.3 min shows characteristic mass information for probe **1**, while the new peak at 8.0 min shows mass information for **BNM153** (Fig. S4 in the Supporting

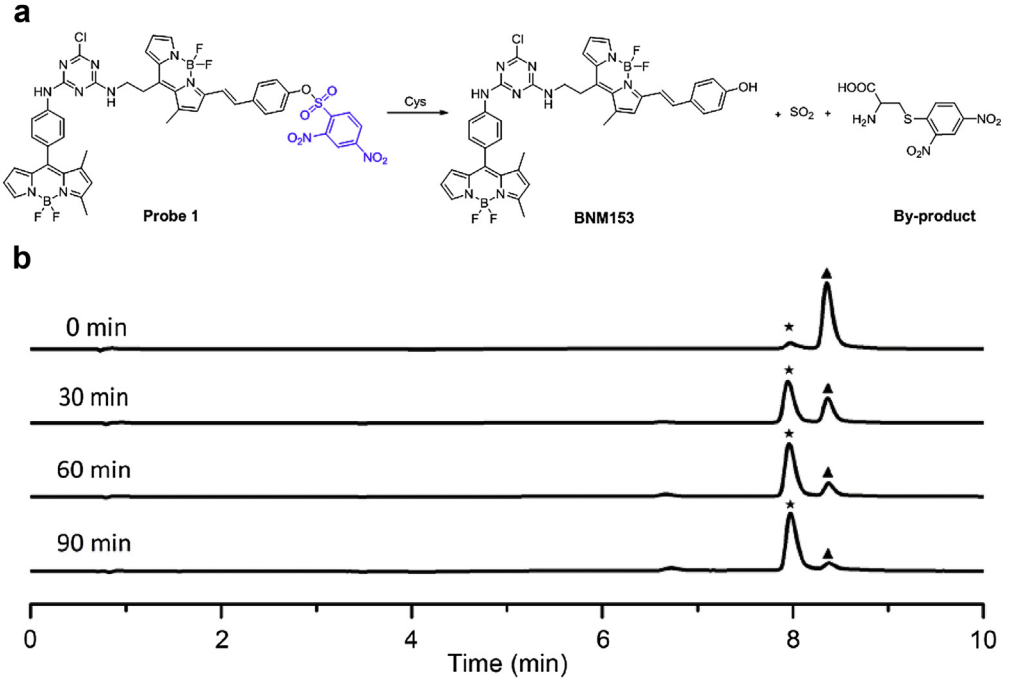


**Fig. 6.** (a) Proposed sensing mechanism; (b) HPLC-MS spectral changes for probe **1** upon addition of Cys (from 0 min to 90 min, UV detection: 560 nm).

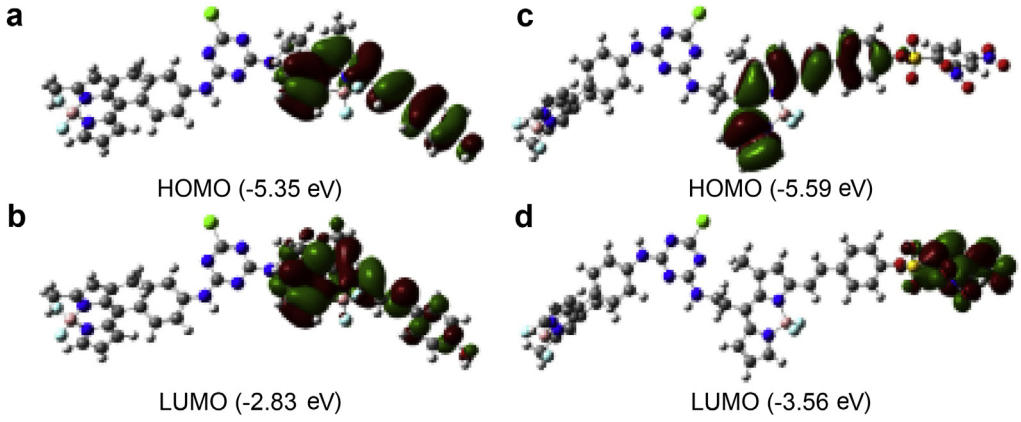


**Fig. 7.** The frontier molecular orbitals (MOs) of **BNM153** and probe **1**. (a) the HOMO of **BNM153**, (b) the LUMO of **BNM153**, (c) the HOMO of probe **1** and (d) the LUMO of probe **1**. The energy levels of the MOs are shown (eV). Calculations are based on ground state geometry by DFT at the B3LYP/6-31G(d)/level using Gaussian 09.

Information). Further characterization shows that another new peak which appeared at 4.9 min was proven to be a by-product (Fig. S5 in the Supporting Information). Taken together, the results have successfully demonstrated that probe **1** when in response to Cys forms the precursor **BNM153**.

Meanwhile, density functional theory (DFT) calculations were carried out to elucidate the mechanism of fluorescence enhancement when **BNM153** formation was observed after the addition of Cys to probe **1**. The excited state related calculations were carried out with the time-dependent DFT (TDDFT), based on the optimized ground state geometry. From the calculated data, both HOMO and LUMO of **BNM153** are localized on the π-conjugated acceptor part, and the HOMO−1 and LUMO+1 are localized on the donor BODIPY part (Fig. 7 and Fig. S6 in the Supporting Information). Also, from the calculated energy, two main allowed electronic transition were observed for **BNM153**, which are H−1 → L + 1, 402 nm, $f = 0.6936$ and H → L, 461 nm, $f = 0.6895$ (Table 2). These calculation results indicated two main absorption bands of **BNM153**. The calculated oscillator strength ($f$) for the HOMO to LUMO transition is 1.1342, which indicates that radioactive decay is possible and eventually leads to emission of **BNM153** [25].

At the same time, the HOMO of probe **1** is localized from the BODIPY part of the acceptor onto the phenylethylene linker (C═C), whereas the LUMO of probe **1** is localized on DNBS moiety. The HOMO to LUMO transition is composed of a full electron-transfer process from acceptor BODIPY to the electron-withdrawing DNBS moiety. The calculated oscillator strength ($f$) for this transition is only 0.004. This means that the direct HOMO to LUMO transition is forbidden, thus LUMO to HOMO is a non-radioactive transition [23,34–37]. These predictions are in full agreement with the experimental results and clearly demonstrate the reasons for the photoproperties of probe **1** and the precursor **BNM153**. Furthermore, the calculated red shift from probe **1** to **BNM153** (6 nm) matches well with the experimental data (9 nm). This concordant calculated data provides strong support for the proposed mechanism for probe **1**.

**Table 2**
Selected parameters for the vertical excitation (UV-vis absorptions) of the compounds. Electronic excitation energies (eV) and oscillator strengths ($f$), configurations of the low-lying excited status of the probe **1** and **BNM153**. Calculated by TDDFT//B3LYP/6-31G(d), based on the optimized ground state geometries.

| | TDDFT//CAM-B3LYP/6-31G(d) | | | |
|---|---|---|---|---|
| | Energy[a] | $f$[b] | Composition[c] | CI[d] |
| **BNM153** | 2.6887 eV (461.14 nm) | 1.1342 | H → L | 0.68946 |
| | 3.0837 eV (402.06 nm) | 0.4788 | H−1 → L + 1 | 0.69358 |
| Probe **1** | 2.7202 eV (455.79 nm) | 1.0094 | H → L + 1 | 0.69348 |
| | 3.0783 eV (402.76 nm) | 0.4734 | H−1 → L + 2 | 0.68706 |
| | 3.5597 eV (348.29 nm) | 0.004 | H → L | 0.60272 |

[a] Only selected excited states were considered. The numbers in parentheses are the excitation energy in wavelength.
[b] Oscillator strength.
[c] H stands for HOMO and L stands for LUMO. Only the main configurations are presented.
[d] Coefficient of the wavefunction for each excitations. The CI coefficients are in absolute values.

### 3.5. Application of probe 1 in fluorescent imaging of cellular thiols

Considering the excellent sensing performance of probe **1** towards Cys and Hcy, we decided to employ probe **1** for the fluorescence imaging of cellular thiols (Fig. 8). After incubating HeLa cells with probe **1** at 37 °C for 30 min, an obvious fluorescence was observed inside the cells. To validate the finding that this fluorescence turn-on was specific due to the cellular thiols, a control experiment was performed, where HeLa cells were first incubated with N-methylmaleimide (NMM) at 37 °C for 30 min to remove cellular thiols prior to incubation with probe **1**. The results show that when NMM was used, almost no fluorescence was observed inside the cells, suggesting that fluorescence signal observed in Fig. 8b is most likely due to the reaction of probe **1** with intracellular thiol species.

To eliminate possible interference by GSH during intracellular Cys detection, HeLa cells were treated with L-buthionine sulfoximine (BSO), prior to imaging with probe **1**. Unlike NMM which does not differentiate between Cys, Hcy or GSH, but lowers concentration of cellular thiols in general, BSO selectively inhibits γ−glutamylcysteine synthetase [38]. As such, it is expected that addition of BSO precludes replenishment of GSH from Cys, hence, lowering the effective concentration of GSH within the cells under the conditions of oxidative stress. In fact, the fluorescence intensity of probe **1** was decreased with BSO−$H_2O_2$ pre-treatment and recovered by the addition of L-Cys (Fig. 9 and Fig. S7 in the Supporting Information). On this note, we thus believe that the fluorescence signal from the cells is associated with changes in intracellular Cys concentration rather than with GSH. Moreover, considering the much lower intracellular concentration of Hcy, probe **1** can be used for monitoring changes of the cellular Cys concentration.

## 4. Conclusions

By introducing the electron-withdrawing group 2,4-dinitrobenzenesulfonyl (DNBS) to the end of the FRET-based

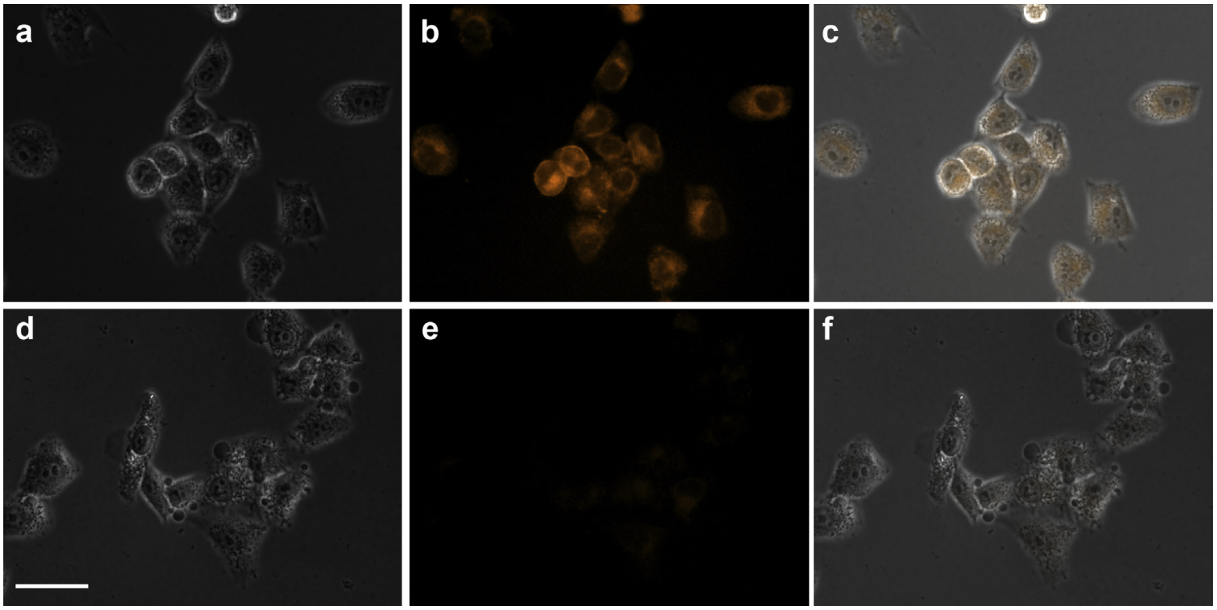


**Fig. 8.** Fluorescent microscopic images of HeLa cells. (a–c) Images of cells incubated with probe **1** (3 μM) for 30 min at 37 °C. (d–f) Images of cells pre-treated with *N*-methylmaleimide (1 mM) for 30 min and then incubated with probe **1** (3 μM) for 30 min at 37 °C; (a) and (d) represent the corresponding phase contrast images of (b) and (e), respectively; (c) and (f) represent the corresponding merged images of (a, b) and (d, e), respectively. Images were taken with a 40× objective. Scale bar represents 50 μm.

BODIPY fluorophore, we constructed a turn-on Cys and Hcy sensor. The unique photophysical properties of precursor of probe **1**, such as high ability for light harvesting, no fluorescence leaks from the donor, high quantum yield and large pseudo-Stokes shifts, features attracts us to synthesize probe **1** to be a new candidate for cellular thiols probe. HPLC-MS study and DFT calculations give strong support for the mechanism of Cys detection by probe **1**. Furthermore, bioimaging results show that probe **1** can easily penetrate cell membrane for detection of thiol species in living cells. Altogether, these results indicate that probe **1** is a good candidate for biothiol detection in living cells.

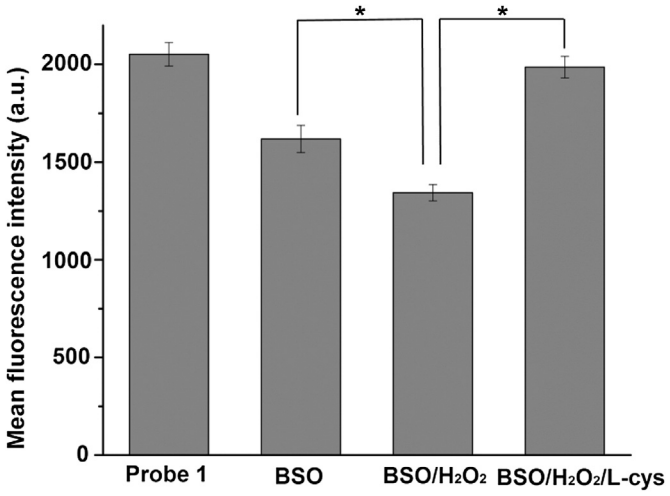


**Fig. 9.** Fluorescent intensity measurements of HeLa cells. Cells were pre-treated with 1 mM L-buthionine sulfoximine (BSO) or 1 mM BSO and 0.1 mM $H_2O_2$ for 1 h. Cells from latter incubation were further treated with 1 mM L-cysteine (L-cys) for 1 h or left untreated before incubation with probe (3 μM) for 30 min. As control, cells were incubated with probe **1** only. Fluorescence intensities were displayed as averages of measurements from three sites. $^*p < 0.005$.

## Acknowledgements

This study was supported by an intramural funding from A*STAR (Agency for Science, Technology and Research, Singapore) Biomedical Research Council and a Singapore Ministry of Education Academic Research Fund Tier 2 (MOE2010-T2-2-030).

## Appendix A. Supplementary data

Supplementary data related to this article can be found at http://dx.doi.org/10.1016/j.biomaterials.2014.04.035.

## References

[1] Zhang S, Ong CN, Shen HM. Critical roles of intracellular thiols and calcium in parthenolide-induced apoptosis in human colorectal cancer cells. Cancer Lett 2004;208:143–53.
[2] Jung HS, Chen X, Kim JS, Yoon J. Recent progress in luminescent and colorimetric chemosensors for detection of thiols. Chem Soc Rev 2013;42:6019–31.
[3] Shahrokhian S. Lead phthalocyanine as a selective carrier for preparation of a cysteine-selective electrode. Anal Chem 2001;73:5972–8.
[4] Seshadri S, Beiser A, Selhub J, Jacques PF, Rosenberg IH, D'Agostino RB, et al. Plasma homocysteine as a risk factor for dementia and Alzheimer's disease. N Engl J Med 2002;346:476–83.
[5] Vacek J, Klejdus B, Petrlova J, Lojkova L, Kuban V. A hydrophilic interaction chromatography coupled to a mass spectrometry for the determination of glutathione in plant somatic embryos. Analyst 2006;131:1167–74.
[6] Ling YY, Yin XF, Fang ZL. Simultaneous determination of glutathione and reactive oxygen species in individual cells by microchip electrophoresis. Electrophoresis 2005;26:4759–66.
[7] Calvo-Marzal P, Chumbimuni-Torres KY, Hoehr NF, Kubota LT. Determination of glutathione in hemolysed erythrocyte with amperometric sensor based on TTF-TCNQ. Clin Chim Acta 2006;371:152–8.
[8] Zhai D, Lee SC, Yun SW, Chang YT. A ratiometric fluorescent dye for the detection of glutathione in live cells and liver cancer tissue. Chem Commun 2013;49:7207–9.
[9] Niu LY, Guan YS, Chen YZ, Wu LZ, Tung CH, Yang QZ. BODIPY-based ratiometric fluorescent sensor for highly selective detection of glutathione over cysteine and homocysteine. J Am Chem Soc 2012;134:18928–31.
[10] Niu LY, Guan YS, Chen YZ, Wu LZ, Tung CH, Yang QZ. A turn-on fluorescent sensor for the discrimination of cystein from homocystein and glutathione. Chem Commun 2013;49:1294–6.
[11] Jung HS, Han JH, Pradhan T, Kim S, Lee SW, Sessler JL, et al. A cysteine-selective fluorescent probe for the cellular detection of cysteine. Biomaterials 2012;33:945–53.

[12] Jung HS, Pradhan T, Han JH, Heo KJ, Lee JH, Kang C, et al. Molecular modulated cysteine-selective fluorescent probe. Biomaterials 2012;33:8495–502.
[13] Yang XF, Guo YX, Strongin RM. A seminaphthofluorescein-based fluorescent chemodosimeter for the highly selective detection of cysteine. Org Biomol Chem 2012;10:2739–41.
[14] Zhou X, Jin X, Sun G, Wu X. A sensitive and selective fluorescent probe for cysteine based on a new response-assisted electrostatic attraction strategy: the role of spatial charge configuration. Chem Eur J 2013;19:7817–24.
[15] Hu MM, Fan JL, Li HL, Song KD, Wang S, Cheng GH, et al. Fluorescent chemodosimeter for Cys/Hcy with a large absorption shift and imaging in living cells. Org Biomol Chem 2011;9:980–3.
[16] Lee KS, Kim TK, Lee JH, Kim HJ, Hong JI. Fluorescence turn-on probe for homocysteine and cysteine in water. Chem Commun; 2008:6173–5.
[17] Li HL, Fan JL, Wang JY, Tian MZ, Du JJ, Sun SG, et al. A fluorescent chemodosimeter specific for cysteine: effective discrimination of cysteine from homocysteine. Chem Commun; 2009:5904–6.
[18] Wang P, Liu J, Lv X, Liu YL, Zhao Y, Guo W. A naphthalimide-based glyoxal hydrazone for selective fluorescence turn-on sensing of Cys and Hcy. Org Lett 2012;14:520–3.
[19] Jiang XD, Zhang J, Shao XM, Zhao WL. A selective fluorescent turn-on NIR probe for cysteine. Org Biomol Chem 2012;10:1966–8.
[20] Li X, Qian SJ, He QJ, Yang B, Li J, Hu YZ. Design and synthesis of a highly selective fluorescent turn-on probe for thiol bioimaging in living cells. Org Biomol Chem 2010;8:3627–30.
[21] Liu XD, Sun R, Ge JF, Xu YJ, Xu Y, Lu JM. A squaraine-based red emission off-on chemosensor for biothiols and its application in living cells imaging. Org Biomol Chem 2013;11:4258–64.
[22] Lu JX, Sun CD, Chen W, Ma HM, Shi W, Li XH. Determination of non-protein cysteine in human serum by a designed BODIPY-based fluorescent probe. Talanta 2011;83:1050–6.
[23] Shao JY, Guo HM, Ji SM, Zhao JZ. Styryl-BODIPY based red-emitting fluorescent OFF-ON molecular probe for specific detection of cysteine. Biosens Bioelectron 2011;26:3012–7.
[24] Wei M, Yin P, Shen Y, Zhang L, Deng J, Xue S, et al. A new turn-on fluorescent probe for selective detection of glutathione and cysteine in living cells. Chem Commun 2013;49:4640–2.
[25] Shao JY, Sun HY, Guo HM, Ji SM, Zhao JZ, Wu WT, et al. A highly selective red-emitting FRET fluorescent molecular probe derived from BODIPY for the detection of cysteine and homocysteine: an experimental and theoretical study. Chem Sci 2012;3:1049–61.
[26] Long LL, Lin WY, Chen BB, Gao WS, Yuan L. Construction of a FRET-based ratiometric fluorescent thiol probe. Chem Commun 2011;47:893–5.
[27] Zhang XL, Xiao Y, Qian XH. A ratiometric fluorescent probe based on FRET for imaging $Hg^{2+}$ ions in living cells. Angew Chem Int Ed 2008;47:8025–9.
[28] Lin WY, Yuan L, Cao ZM, Feng YM, Song JZ. Through-bond energy transfer cassettes with minimal spectral overlap between the donor emission and acceptor absorption: coumarin-rhodamine dyads with large pseudo-Stokes shifts and emission shifts. Angew Chem Int Ed 2010;49:375–9.
[29] Arbeloa FL, Ojeda PR, Arbeloa IL. Fluorescence self-quenching of the molecular-forms of rhodamine-B in aqueous and ethanolic solutions. J Lumin 1989;44:105–12.
[30] Frisch MJ, Trucks GW, Schlegel HB, Scuseria GE, Robb MA, Cheeseman JR, et al. Gaussian 09, revision A.01. Wallingford, CT: Gaussian, Inc.; 2009.
[31] Vendrell M, Krishna GG, Ghosh KK, Zhai DT, Lee JS, Zhu Q, et al. Solid-phase synthesis of BODIPY dyes and development of an immunoglobulin fluorescent sensor. Chem Commun 2011;47:8424–6.
[32] Kang NY, Lee SC, Park SJ, Ha HH, Yun SW, Kostromina E, et al. Visualization and isolation of langerhans islets by a fluorescent probe PiY. Angew Chem Int Ed 2013;52:8557–60.
[33] Tang Y, Yang HR, Sun HB, Liu SJ, Wang JX, Zhao Q, et al. Rational design of an "OFF-ON" phosphorescent chemodosimeter based on an iridium(III) complex and its application for time-resolved luminescent detection and bioimaging of cysteine and homocysteine. Chem Eur J 2013;19:1311–9.
[34] Guo H, Jing Y, Yuan X, Ji S, Zhao J, Li X, et al. Highly selective fluorescent OFF-ON thiol probes based on dyads of BODIPY and potent intramolecular electron sink 2,4-dinitrobenzenesulfonyl subunits. Org Biomol Chem 2011;9:3844–53.
[35] Ji S, Yang J, Yang Q, Liu S, Chen M, Zhao J. Tuning the intramolecular charge transfer of alkynylpyrenes: effect on photophysical properties and its application in design of OFF-ON fluorescent thiol probes. J Org Chem 2009;74:4855–65.
[36] Ji S, Guo H, Yuan X, Li X, Ding H, Gao P, et al. A highly selective OFF-ON red-emitting phosphorescent thiol probe with large stokes shift and long luminescent lifetime. Org Lett 2010;12:2876–9.
[37] Kowalczyk T, Lin Z, Van Voorhis T. Fluorescence quenching by photoinduced electron transfer in the $Zn^{2+}$ sensor zinpyr-1: a computational investigation. J Phys Chem A 2010;114:10427–34.
[38] Deneke SM, Fanburg BL. Regulation of cellular glutathione. Am J Physiol 1989;257:L163–73.